New Phytologist

Historical changes in the stomatal limitation of photosynthesis: empirical support for an optimality principle

Aliénor Lavergne[1,2], Steve Voelker[3], Adam Csank[4], Heather Graven[2,5], Hugo J. de Boer[6], Valérie Daux[7], Iain Robertson[8], Isabel Dorado-Liñán[9], Elisabet Martínez-Sancho[10], Giovanna Battipaglia[11], Keith J. Bloomfield[1], Christopher J. Still[12], Frederick C. Meinzer[13], Todd E. Dawson[14], J. Julio Camarero[15], Rory Clisby[8], Yunting Fang[16], Annette Menzel[17], Rachel M. Keen[18], John S. Roden[19] and I. Colin Prentice[1,5,20,21]

[1]Department of Life Sciences, Imperial College London, Silwood Park Campus, Buckhurst Road, Ascot, SL5 7PY, UK; [2]Department of Physics, Imperial College London, Exhibition Road, London, SW7 2AZ, UK; [3]Department of Environmental and Forest Biology, SUNY College of Environmental Science and Forestry, Syracuse, NY 13210, USA; [4]Department of Geography, University of Nevada-Reno, 1664 N. Virginia St, Reno, NV 89557, USA; [5]Grantham Institute – Climate Change and the Environment, Imperial College London, Exhibition Road, London, SW7 2AZ, UK; [6]Department of Environmental Sciences, Utrecht University, 3584 CB, Utrecht, the Netherlands; [7]Laboratoire des Sciences du Climat et de l'Environnement, CEA-CNRS-UVSQ, 91191 Gif-sur-Yvette, France; [8]Department of Geography, Swansea University, Swansea, SA2 8PP, UK; [9]Forest Genetics and Ecophysiology Research Group, Technical University of Madrid, Madrid 28040, Spain; [10]Swiss Federal Institute for Forest, Snow and Landscape Research WSL, Zürcherstrasse 111, Birmensdorf 8903, Switzerland; [11]Department of Environmental, Biological and Pharmaceutical Sciences and Technologies, University of Campania "L. Vanvitelli", Via Vivaldi, 81100, Caserta, Italy; [12]Department of Forest Ecosystems & Society, Oregon State University, Corvallis, OR 97331-5704, USA; [13]USDA Forest Service, Pacific Northwest Research Station, Corvallis, OR 97331-8550, USA; [14]Department of Integrative Biology, University of California – Berkeley, Berkeley, CA 94720-3200, USA; [15]Instituto Pirenaico de Ecología (IPE-CSIC), E-50192, Zaragoza, Spain; [16]Institute of Applied Ecology, Chinese Academy of Sciences, Shenyang 110016, China; [17]Ecoclimatology, Department of Ecology and Ecosystem Management, Technical University of Munich, 85354, Freising, Germany; [18]Division of Biology, Kansas State University, Manhattan, KS 66506, USA; [19]Department of Biology, Southern Oregon University, Ashland, OR 97520, USA; [20]Department of Biological Sciences, Macquarie University, North Ryde, NSW 2109, Australia; [21]Department of Earth System Science, Tsinghua University, Beijing 100084, China

Author for correspondence:
Aliénor Lavergne
Tel: +44 77 5 15 60400
Email: a.lavergne@imperial.ac.uk

Received: *12 July 2019*
Accepted: *31 October 2019*

New Phytologist (2020) **225:** 2484–2497
doi: 10.1111/nph.16314

Key words: leaf-internal CO_2 concentration, least-cost hypothesis, optimality, stable carbon isotopes, tree rings, water-use efficiency.

Summary

- The ratio of leaf internal (c_i) to ambient (c_a) partial pressure of CO_2, defined here as χ, is an index of adjustments in both leaf stomatal conductance and photosynthetic rate to environmental conditions. Measurements and proxies of this ratio can be used to constrain vegetation model uncertainties for predicting terrestrial carbon uptake and water use.
- We test a theory based on the least-cost optimality hypothesis for modelling historical changes in χ over the 1951–2014 period, across different tree species and environmental conditions, as reconstructed from stable carbon isotopic measurements across a global network of 103 absolutely dated tree-ring chronologies. The theory predicts optimal χ as a function of air temperature, vapour pressure deficit, c_a and atmospheric pressure.
- The theoretical model predicts 39% of the variance in χ values across sites and years, but underestimates the intersite variability in the reconstructed χ trends, resulting in only 8% of the variance in χ trends across years explained by the model.
- Overall, our results support theoretical predictions that variations in χ are tightly regulated by the four environmental drivers. They also suggest that explicitly accounting for the effects of plant-available soil water and other site-specific characteristics might improve the predictions.

Introduction

The net uptake of atmospheric CO_2 by the terrestrial biosphere, which acts as a sink for about 30% of anthropogenic CO_2 emissions, has helped to reduce the increase in atmospheric CO_2 concentration – and therefore dampened climate change – since the beginning of the industrial era (Le Quéré *et al.*, 2018). However, it is still unclear how atmospheric CO_2, climate, and other environmental changes will influence the future strength of the terrestrial carbon (C) sink (Ciais *et al.*, 2013; Ballantyne *et al.*, 2015; Schimel *et al.*, 2015). It has been suggested that the magnitude of net terrestrial C uptake is likely to decline in the future through various mechanisms, including resource limitations on the CO_2 'fertilization' effect as a result of nitrogen (N) availability (Reich *et al.*, 2006; Reich & Hobbie, 2013), reduced water availability as a result of changes in the hydrological cycle (Zhao & Running, 2010; Humphrey *et al.*, 2018; Green *et al.*, 2019), or enhanced turnover of soil C as a result of warming (Knorr

et al., 2005; Li *et al.*, 2018). Yet, the extent to which these processes might affect the terrestrial C sink is still largely unknown, especially when considering the real possibility of plant adaptation and acclimation that may occur over decadal to longer timescales. Current models of the terrestrial biosphere incorporate different formulations of the underlying processes, including photosynthesis and leaf gas exchange responses to varying CO_2 concentrations (Rogers *et al.*, 2017), the impact of soil moisture stress on photosynthesis and stomatal conductance (De Kauwe *et al.*, 2013), and C allocation and turnover (De Kauwe *et al.*, 2014), leading to large differences in simulated terrestrial CO_2 uptake and future climate change. New metrics and proxies of key biological processes are thus needed to improve and reduce uncertainties in terrestrial models.

The ratio of leaf internal (c_i) to ambient (c_a) partial pressure of CO_2 (hereafter termed χ) is a key metric of physiological function in plant leaves being determined by both stomatal conductance in the short term and photosynthetic biochemical capacity at longer timescales (Farquhar *et al.*, 1982). Thus, χ is the key variable for the study of C uptake. Under some conditions it can also provide insights into changes in intrinsic water-use efficiency (iWUE), that is, the ratio of photosynthesis to stomatal conductance, defined as $iWUE = c_a\ (1-\chi)/1.6$ (Ehleringer *et al.*, 1993). As there are many other definitions of water-use efficiency (WUE) by plants, each with different meanings (Lavergne *et al.*, 2019), analysis of data directly in terms of χ is preferred here. Plants assimilate the heavier $^{13}CO_2$ molecules less readily than $^{12}CO_2$ because of their slower diffusion through the stomata and preferential fixation of $^{12}CO_2$ by Rubisco, resulting in a discrimination against ^{13}C compared with ^{12}C, defined as $\Delta^{13}C$ (Park & Epstein, 1960). In C_3 plants, $\Delta^{13}C$ is principally determined by χ. Thus, reconstructing long-term effective values of χ from $\Delta^{13}C$ derived from the stable isotope $^{13}C/^{12}C$ ratio ($\delta^{13}C$) measured in plant materials (including tree rings), or even in atmospheric CO_2, can offer valuable insights into stomatal and photosynthetic adjustments to environmental conditions. As air masses are transported and mixed rapidly in the turbulent lower atmosphere, $\Delta^{13}C$ values inferred from atmospheric $\delta^{13}CO_2$ are representative of processes occurring at regional (Ballantyne *et al.*, 2010; Peters *et al.*, 2018) or global (Keeling *et al.*, 2017) scales, while values derived from $\delta^{13}C$ measured in tree rings reflect ecophysiological processes at the individual plant level. Thus, $\delta^{13}C$ data from different sources can, in principle, be used to evaluate and improve the representation of stomatal and photosynthetic behaviour in models at different spatial scales. However, atmospheric $\delta^{13}CO_2$ is also influenced by many other processes, such as ocean–atmosphere gas exchange and isotope disequilibrium fluxes (Keeling *et al.*, 2017), complicating the derivation of long-term changes in χ using atmospheric data.

Formulations for $\Delta^{13}C$ have been included in vegetation models (Saurer *et al.*, 2014; Frank *et al.*, 2015; Raczka *et al.*, 2016; Keller *et al.*, 2017) and evaluated using existing observations as recommended by the Coupled Model Intercomparison Project Phase 6 (CMIP6), which coordinates current Earth system modelling activities internationally (Eyring *et al.*, 2016; Jones *et al.*, 2016). Yet some recent studies have shown that current models overestimate the decrease in $\Delta^{13}C$ (and the associated increase in WUE) over the 20th century (Keller *et al.*, 2017) or simulate an increase in both $\Delta^{13}C$ and WUE at leaf level, which is inconsistent with biological theory (Raczka *et al.*, 2016). These studies demonstrate that $\Delta^{13}C$ can reveal explicit biases within the models. Errors in the simulation of $\Delta^{13}C$ can, however, be difficult to attribute to particular processes. Incomplete, empirical descriptions of the processes determining χ in vegetation models and incorrect assumptions about key parameters in the model of photosynthesis may cause discrepancies between observed and predicted $\Delta^{13}C$. Many models assign fixed parameter values to different plant functional types (PFTs) (Rogers *et al.*, 2017), but this approach overlooks the ability of plants (within any one PFT) to acclimate or adapt to environmental changes (Wullschleger *et al.*, 2014; Martínez-Sancho *et al.*, 2018; Dorado-Liñán *et al.*, 2019). Also, some of the processes linking c_i to $\Delta^{13}C$ have been neglected. The potential impact of fractionations during the transport of CO_2 from the intercellular space to the chloroplasts and during photorespiration have been described (Ubierna & Farquhar, 2014), and may be important to include when analysing historical trends (Seibt *et al.*, 2008; Keeling *et al.*, 2017; Schubert & Jahren, 2018; Lavergne *et al.*, 2019). Accordingly, there is a need to probe the assumptions about leaf gas exchange incorporated into such models, to include the known physiological and environmental processes influencing $\Delta^{13}C$, and to evaluate the resulting simulations with long-term stable C isotope data.

Simpler analytical models can provide an integrative approach to understanding whole-plant responses to environmental changes via the general hypothesis that plants optimize their physiology towards maximizing fitness (Medlyn *et al.*, 2013; Dewar *et al.*, 2018). However, the tradeoff between the benefits and costs of stomatal opening (C gain at the expense of water loss) and investments in photosynthetic biochemistry (requiring N and energy) is still not completely understood; in particular, the specific nature of the costs remains an open question. Different optimization hypotheses for the control of stomatal conductance have been proposed – reviewed in Buckley (2017) and Dewar *et al.* (2018) – that make different predictions of stomatal responses to the environment. The Cowan–Farquhar optimality hypothesis states that leaves maximize the difference between photosynthesis and the C cost of transpiration, that is, $A - E/\lambda$, where A is the photosynthesis rate, E is the rate of transpiration and λ is an 'exchange rate' between C and water (Cowan & Farquhar, 1977; Katul *et al.*, 2010; Buckley & Schymanski, 2014; Sperry *et al.*, 2017). λ has usually been determined as a function of soil moisture (Manzoni *et al.*, 2013) and of xylem water potential (Wolf *et al.*, 2016; Sperry *et al.*, 2017). The Cowan–Farquhar optimality hypothesis, however, does not account for the costs of maintaining both water flow and photosynthetic capacity (Givnish, 1986). Following the least-cost optimality hypothesis proposed by Wright *et al.* (2003), Prentice *et al.* (2014) introduced the alternative criterion that leaves minimize the summed unit costs of transpiration and carboxylation, that is, $(a_E E + b_V V_{cmax})/A$, where a_E is the sapwood maintenance cost per unit of transpiration capacity and b_V is the cost associated

with the maintenance of photosynthetic (carboxylation) capacity (V_{cmax}) (Rogers, 2014). Dewar *et al.* (2018) analysed another criterion, following Givnish (1986), whereby the cost of stomatal opening arises from nonstomatal reductions in photosynthesis induced by leaf water stress. The authors explored different hypotheses in which reduced leaf water potential leads to a reduction in either V_{cmax} or mesophyll conductance. Predicted stomatal responses were broadly similar to those derived from the least-cost optimality hypothesis (Dewar *et al.*, 2018), although the reduction of V_{cmax} rather than mesophyll conductance provided a better fit across different PFTs (Gimeno *et al.*, 2019).

Here we test the theoretical framework implied by the least-cost optimality hypothesis for predicting long-term changes in χ across the globe, during a period of steadily increasing c_a (*c.* 85 ppm over 1951–2014). Spatial patterns of χ predicted by the least-cost hypothesis have been supported by analyses of leaf $\Delta^{13}C$ data at the regional (Bloomfield *et al.*, 2019) and global scales (Wang *et al.*, 2017b). However, simulations of χ and its trends over recent decades using this model still await evaluation against long-term observations. Here we first reconstruct changes in χ over 1951–2014 using a global tree-ring $\delta^{13}C$ ($\delta^{13}C_{TR}$) network of 103 sites. We then compare model predictions and reconstructions for their spatial and temporal patterns and examine the sensitivity of predicted and isotope-derived χ to the environmental drivers of the model and other constraints. Our aim is to address the following questions: can temporal variations in χ – as indexed by long-term $\delta^{13}C_{TR}$ measurements – be predicted by the least-cost hypothesis; how well do these predictions of χ reproduce the ratio's observed dependency on environmental drivers; and are there any other potential environmental controls on χ that should be considered in order to improve these predictions?

Materials and Methods

Observational dataset of χ

We compiled 103 absolutely dated $\delta^{13}C_{TR}$ chronologies from published and unpublished materials representing different PFTs (deciduous broadleaf forest (DBF, $n = 29$) and evergreen needleleaf forest (ENF, $n = 74$)) and environmental contexts in the temperate and boreal zones, with at least 30 yr of records over the 1951–2014 period when most data were available (Fig. 1; Supporting Information Table S1; Dataset S1). $\delta^{13}C_{TR}$ (i.e. the ratio of ^{13}C to ^{12}C of the wood component compared with an internationally accepted standard material) was derived from cellulose (with just two exceptions where bulk wood was used) and from either the whole ring (WR, $n = 65$; including both earlywood and latewood) or only latewood (LW, $n = 38$; Table S1). The analytical error in the $\delta^{13}C_{TR}$ measurements was typically ± 0.15‰. $\Delta^{13}C$ for each series was calculated as:

$$\Delta^{13}C = \frac{\delta^{13}CO_2 - (\delta^{13}C_{TR} - d)}{1 + (\delta^{13}C_{TR} - d)/1000} \quad \text{Eqn 1}$$

where $\delta^{13}CO_2$ is the stable isotopic composition of atmospheric CO_2 in the year of ring formation, and d (‰) quantifies the sum of discriminations beyond those associated with the production of the primary photosynthetic assimilates: 1.9‰ between leaf organic matter and bulk wood (Badeck *et al.*, 2005), and 2.1 ± 1.2‰ between leaf organic matter and α-cellulose (Frank *et al.*, 2015). For each year, $\Delta^{13}C$ was used to derive χ_{iso} (i.e. the isotope-derived χ) with the model from Farquhar *et al.* (1982) including an explicit fractionation term for photorespiration as recommended by several studies (e.g. Ubierna & Farquhar, 2014; Schubert & Jahren, 2018; Lavergne *et al.*, 2019) but assuming effectively infinite boundary layer and mesophyll conductances, and negligible fractionation during mitochondrial respiration (Ghashghaie *et al.*, 2003; Evans & Von Caemmerer, 2013):

$$\Delta^{13}C = a + (b - a)\chi_{iso} - f\frac{\Gamma^*}{c_a} \quad \text{Eqn 2}$$

where a, b and f represent isotope fractionations as a result of CO_2 diffusion in air (4.4‰; Craig, 1953), effective Rubisco carboxylation (26–30‰) and photorespiration (8–16‰; Ubierna & Farquhar, 2014), respectively. Γ^* (Pa) is the CO_2 compensation point in the absence of mitochondrial respiration, that is, the value of c_i at which the rate of photosynthetic CO_2 uptake equals that of photorespiratory CO_2 evolution, calculated from the temperature and pressure response, $\Gamma^* = \Gamma^*_{25}\ P_{atm}/P_0 \exp[\Delta H_a(T - 298)/(RT \times 298)]$, with Γ^*_{25} the photorespiratory compensation point at 25°C, ΔH_a the activation energy for Γ^* (Bernacchi *et al.*, 2001), T the temperature, R the universal gas constant (Moldover *et al.*, 1988), and P_{atm} and P_0 the ambient and sea-level atmospheric pressures, respectively. Note that we did not consider mesophyll conductance (g_m) in our calculations because information on g_m, which is highly variable between species (von Caemmerer & Evans, 2015) and may fluctuate over long time periods (Flexas *et al.*, 2008), is generally lacking. Nevertheless, given the influence of g_m in the full discrimination model, we provide a sensitivity analysis in the Supporting Information (Notes S1; Fig. S1).

From Eqns 1 and 2, χ_{iso} can be written as:

$$\chi_{iso} = \frac{\left(\frac{\delta^{13}CO_2 - (\delta^{13}C_{TR} - d)}{1 + (\delta^{13}C_{TR} - d)/1000}\right) - a + f\frac{\Gamma^*}{c_a}}{b - a} \quad \text{Eqn 3}$$

The choice of the values in Eqn 3 for the fractionation factors related to Rubisco carboxylation (b), photorespiration (f) and postphotosynthetic processes (d) does not affect the trend estimates of χ_{iso} but only modulates the mean χ_{iso} values (Fig. S1). In the following, we have used the mean values from their range of uncertainties of $b = 28$‰ and $f = 12$‰ (Ubierna & Farquhar, 2014). Postphotosynthetic fractionations were assumed equal for all species ($d = 2.1$‰ for cellulose and 1.9‰ for bulk wood) because information quantifying these effects for individual species is sparse (Bowling *et al.*, 2008; Seibt *et al.*, 2008; Wingate *et al.*, 2008; Gessler *et al.*, 2014). Thus, we inevitably made some approximations that may have contributed to uncertainty in the reconstructed χ_{iso} values. Finally, to minimize the potential effect of mixing and turnover of nonstructural carbohydrate pools of

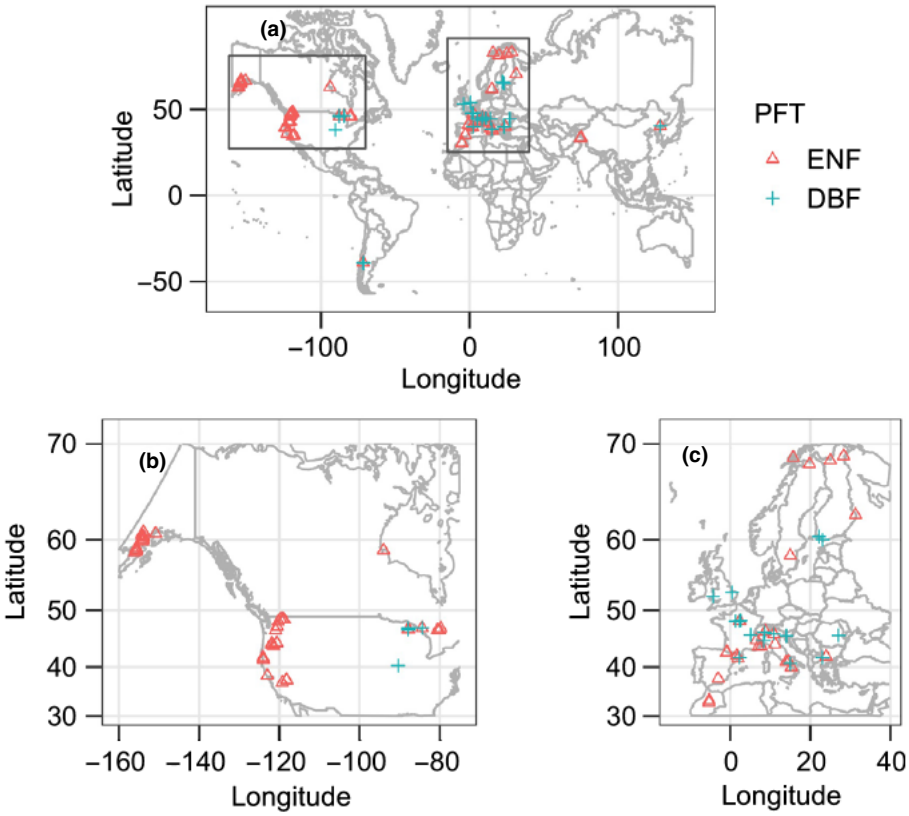

Fig. 1 (a) Location of the selected 103 tree-ring sites with carbon isotopic measurements (see Supporting Information Table S1 for details). Zoom over North America (b) and Europe (c) where the network is denser. Latitude and longitude are in decimal degrees. PFT, plant functional type (deciduous broadleaf forest (DBF, $n = 29$) and evergreen needleleaf forest (ENF, $n = 74$)).

different ages and metabolic history in $\delta^{13}C_{TR}$ (Gessler *et al.*, 2014), we have aggregated the resulting χ_{iso} series into boxcar averages over a 5 yr period.

Prediction of χ following the optimality hypothesis

The theoretical model The theory to predict χ (χ_{pred}, hereafter) following the least-cost optimality hypothesis was introduced (Prentice *et al.*, 2014; Wang *et al.*, 2017b; Stocker *et al.*, 2019a) and applied in several recent studies (Dong *et al.*, 2017; Wang *et al.*, 2017a; Fürstenau Togashi *et al.*, 2018; Bloomfield *et al.*, 2019; Smith *et al.*, 2019). One of the strengths of the model is that there is no distinction among PFTs and biomes, except for the well-established differences between C_3 and C_4 plants, and therefore no fixed parameter defines the behaviour of the vegetation as in most current models (Rogers *et al.*, 2017). Thus, vegetation functions are allowed to evolve freely with environmental changes. The model is driven by P_{atm}, observed air temperature (T), vapour pressure deficit (D) and c_a at the selected time step (here, monthly) as follows:

$$\chi_{pred} = \frac{c_i}{c_a} = \frac{\Gamma^*}{c_a} + \left(1 - \frac{\Gamma^*}{c_a}\right)\frac{\xi}{\xi + \sqrt{D}} \quad \text{Eqn 4a}$$

where

$$\xi = \sqrt{\beta\frac{K + \Gamma^*}{1.6\eta^*}} \quad \text{Eqn 4b}$$

ξ modulates the sensitivity of χ_{pred} to D, β (unitless) is the ratio of cost factors for carboxylation and transpiration (b_V/a_E) at 25°C, η^* (unitless) is the viscosity of water relative to its value at 25°C, and K (Pa) is the effective Michaelis constant for Rubisco-limited photosynthesis at ambient partial pressure of O_2 (O, Pa) given by:

$$K = K_C\left(1 + \frac{O}{K_O}\right) \quad \text{Eqn 5}$$

where K_C (Pa) and K_O (Pa) are the Michaelis constants of Rubisco for carboxylation and oxygenation, respectively. K and η^* are known functions of T and P_{atm}, and can be estimated following Bernacchi *et al.* (2001) and Huber *et al.* (2009), respectively. P_{atm} is calculated from elevation (z) following Allen *et al.* (1998). Only one free parameter is used here, β, whose values were estimated independently for ENF and DBF based on the tree-ring network of $\delta^{13}C$ data using Eqn 4 under the mean environmental conditions over the studied period (see Notes S2; $\beta_{ENF} = 176$ and $\beta_{DBF} = 191$). Note that our assumption of a constant β is a practical approximation based on environmental conditions as β may vary over time (e.g. as a result of changes in soil moisture content; Stocker *et al.*, 2018, 2019b). Thus, the theoretical model does not explicitly account for potential effects of changes in soil moisture on χ (the potential impacts of soil moisture limitation on χ are discussed further in the following). Also, as $c_a > \Gamma^*$ under field conditions, the theory predicts that χ is only slightly dependent on c_a. Overall, optimal χ following the theory is expected to increase with increasing T but to decrease with

increasing D and c_a, and decreasing P_{atm} (i.e. increasing z) (Wang *et al.*, 2017a).

Driving data Latitude and longitude were used to extract minimum and maximum temperatures (T_{min} and T_{max}, °C) and actual vapour pressure (e_a, hPa) for each site from monthly 0.5° resolution data provided by the Climatic Research Unit (CRU TS4.01; Harris *et al.*, 2014). When not provided by the authors (Table S1), z values (km) used to infer P_{atm} were obtained from the WATCH Forcing Data methodology applied to ERA-Interim data (WFDEI) with 0.5° resolution (Weedon *et al.*, 2014) using the latitude and longitude of the site. Estimated z values from the WFDEI dataset were in reasonably good agreement with those provided by authors, when available ($r^2 = 0.77$, $P < 0.001$; Fig. S2). Monthly atmospheric CO_2 concentrations (in ppm) for the 1958–2014 period were derived from *in situ* direct measurements provided by the Scripps Institution of Oceanography (http://scrippsco2.ucsd.edu/data/atmospheric_co2/). For the 1951–1958 period, we interpolated the monthly CO_2 values using the mean seasonal cycle recorded over 1958–2014 and the yearly CO_2 values from a merged product based on ice core data and *in situ* direct measurements (Fig. S3). The c_a dataset was first corrected for the elevation effect and converted into Pa before being used for the analyses as follows: c_a (Pa) $= 10^{-6}\,[CO_2]_{ppm}\,P_{atm}$. Atmospheric $\delta^{13}CO_2$ data for the historical period of interest were extracted from a recent compilation by Graven *et al.* (2017).

We calculated the monthly mean daytime air T ($T_{daytime}$, °C) to consider only the part of the day when photosynthesis occurs, as:

$$T_{daytime} = T_{max}\left\{\frac{1}{2} + \frac{[\sqrt{(1-x^2)}]}{2\arccos x}\right\} + T_{min}\left\{\frac{1}{2} - \frac{[\sqrt{(1-x^2)}]}{2\arccos x}\right\} \quad \text{Eqn 6a}$$

where

$$x = -\tan\phi\tan\delta \quad \text{Eqn 6b}$$

with ϕ the latitude (°) and Δ the average solar declination for the month (Jones, 2013).

Given our hypothesis of infinite boundary layer conductance in Eqn 3, we assumed equality of leaf and air temperatures. Monthly mean daytime D ($D_{daytime}$, kPa) was calculated following Allen *et al.* (1998) using $T_{daytime}$, P_{atm} and monthly mean e_a as:

$$D_{daytime} = 0.611\, e^{\frac{8.635\,T_{daytime}}{237.3 + T_{daytime}}} - 0.10 e_a \frac{P_{atm}}{P_0} \quad \text{Eqn 7}$$

Model evaluation

For evaluating model predictions against reconstructions, the monthly χ_{pred} values initially calculated following Eqn 4 using the monthly mean daytime values of climate predictors (i.e. $T_{daytime}$, $D_{daytime}$) and c_a were aggregated as medians over the most productive months of the growing season to produce the growing-season χ_{pred} series. At each site, the peak growing-season months, when most of the C to build the tree ring is fixed, were estimated based on a literature review (see Table S1). When no information was available, we assumed a growing season centred over summer months, i.e. June–August for the northern hemisphere. We then aggregated the resulting yearly χ_{pred} series as 5 yr boxcar averages before comparing them with independently estimated, also 5-yr-averaged χ_{iso}.

All statistical analyses were conducted in the open-source statistical environment R (R Core Team & R Development Core Team, 2018). We first compared the spatial and temporal patterns of χ between reconstructions and predictions before investigating potential biases in the predictions. The agreement between χ_{pred} and χ_{iso} values was assessed using the adjusted R-squared (R^2_{adj}), the root mean square error (RMSE), the Akaike information criterion (AIC; Akaike, 1973) and the Bayesian information criterion (BIC) using the R package PERFORMANCE (Lüdecke *et al.*, 2019); overall, lower RMSE, AIC and BIC values indicate greater explanatory power. The temporal changes in χ at each site for both reconstructions and predictions were quantified using the Theil-Sen estimator from the R package TREND (Pohlert, 2018), which calculates a trend as the median of the slopes of all lines through pairs of points (Sen, 1968). Before estimating Theil-Sen trends, χ_{pred} and χ_{iso} values were converted into percentages of changes in χ relative to the site mean, in order to make the trends more comparable with each other:

$$\chi(\%) = \frac{\chi_t - \chi_{mean}}{\chi_{mean}} \times 100 \quad \text{Eqn 8}$$

where χ_t and χ_{mean} are the values for χ at the time resolution considered (5 yr) and for the whole 1951–2014 period, respectively. The resulting χ trend estimates were compared between reconstructions and predictions using different linear regression models. We first applied the ordinary least-squares (OLS) method for reducing the residuals in the linear regression and then applied the M-estimators method to perform robust linear regressions (RLM) using the R package MASS (Venables & Ripley, 2002). The M-estimators method is generally less sensitive to outliers than the OLS method. To assess the effect of temporal changes in growing-season average $T_{daytime}$ and $D_{daytime}$ (hereafter T_g and D_g, respectively) on χ trends, we additionally calculated T_g and D_g trends following the same approach as described earlier.

As a further examination of the skill of the least-cost hypothesis, we investigated the relative dependencies of χ_{pred} and χ_{iso} values on the four drivers of the model using multiple linear regression. To do so, we first calculated the logit-transformed χ_{iso} and χ_{pred} values, as logit $\chi = \log_e[\chi/(1-\chi)]$. Logit transformation stabilizes variance in quantities with a (0,1) range and also simplifies the comparison of the sensitivity of χ to environmental variables. We also estimated the model bias (B) in χ predictions at each site as:

$$B = \frac{\chi_{pred} - \chi_{iso}}{\chi_{iso}} \times 100 \quad \text{Eqn 9}$$

Linear regressions of logit χ_{iso}, logit χ_{pred} and B against the four primary drivers (T_g natural log-transformed D_g, c_a and z) as predictors were applied using OLS. The variance explained by each of the fixed effects was calculated via commonality analyses using the R package YHAT (Nimon *et al.*, 2013). We also tested two linear mixed-effect models (Bolker *et al.*, 2009; Zuur *et al.*, 2009) using the R package LME4 (Bates *et al.*, 2015) which included the four fixed effects described earlier but also a random effect related to site to account for site grouping on variance partitioning. One model included only random intercepts, while another included both random intercepts and slopes. The variance explained by the fixed effects and that explained by the entire models, including both fixed and random effects, were also calculated.

Finally, to investigate the potential influences of soil water availability on χ, we tested different multiple linear models of logit χ_{iso} and B which included the primary drivers of the least-cost hypothesis and one index of plant-available soil water as predictors. Three alternative indices of drought severity or soil water availability were tried: a drought index based on climate water balance (the Standardized Precipitation-Evapotranspiration Index, SPEI) inferred from the 0.5° gridded monthly SPEIbase dataset (Beguería *et al.*, 2010); the surface soil moisture content (θ, m^3 m^{-3}) data extracted at each site from the 0.25° resolution product of the European Space Agency Climate Change Initiative (Dorigo *et al.*, 2017); and an estimate of the ratio of actual evapotranspiration to equilibrium evapotranspiration (Priestley–Taylor coefficient, α) calculated at each site using the SPLASH model (Davis *et al.*, 2017) (see Notes S3 for more details).

All linear models were compared using analysis of variance (ANOVA), RMSE, AIC and BIC. The partial residuals of most models were computed using the R package EFFECTS (Fox & Weisberg, 2018) and the respective residual plots were visually examined against environmental variables.

Data and code availability statement

The implementation of the least-cost optimality hypothesis in R is available via the R package RPMODEL (Stocker *et al.*, 2019a). The R code used for all the numerical analyses presented here is available through https://github.com/Alielav/NP_Lavergneetal2019. The isotope-derived and predicted χ data over the 1951–2014 period are provided in Dataset S1. Except for data explicitly specified as available upon request in Table S1, all the tree-ring $\delta^{13}C$ data are available in the Dataset S1.

Results

Model-data comparison of χ values

Over the 1951–2014 period, χ_{pred} and χ_{iso} values were in reasonable agreement ($R^2_{adj} = 0.39$, RMSE = 0.062, AIC = –3015, BIC = –3000, $P < 0.001$; Fig. 2b), but were more consistent for ENF than DBF sites ($R^2_{adj} = 0.38$, RMSE = 0.063, AIC = –2140, BIC = –2126 for ENF vs $R^2_{adj} = 0.21$, RMSE = 0.054, AIC = –907, BIC = –896 for DBF, $P < 0.001$; Fig. 2a). χ_{pred} values from high-elevation sites (i.e. with low P_{atm}) tended to be lower than those from low-elevation sites (i.e. high P_{atm}), although the reconstructed values did not show this distinction as clearly as the predicted values (Fig. 2b).

Model-data comparison of long-term trends in χ

The median χ trends across sites were not significantly different from zero, either for the isotope-based reconstructions (ranging across sites between −1.41 and 1.89% per 5 yr) or for the model predictions (ranging across sites between –0.27 and 0.27% per 5 yr) ($P > 0.20$, Student's t-test; Fig. 3a). These results indicate that on average across sites, both χ_{iso} and χ_{pred} stayed nearly constant while c_a increased by 2.05% per 5 yr. Reconstructed and predicted χ trends were not significantly different ($P = 0.906$, Student's t-test). However, the variability of χ trends between sites was larger in χ_{iso} than in χ_{pred} (interquartile range = 0.60 vs 0.12; $P < 0.001$, F-test). No significant differences in χ_{iso} trends were detected between ENF and DBF series or between latewood and whole ring series ($P > 0.40$, Student's t-test). χ trends tended to be lower at sites with increased T_g and D_g, but these differences were only significant for the predicted trends (Fig. 3c,d). Predicted and isotope-derived historical χ trends were only slightly related to each other for all sites ($R^2_{adj} = 0.08$,

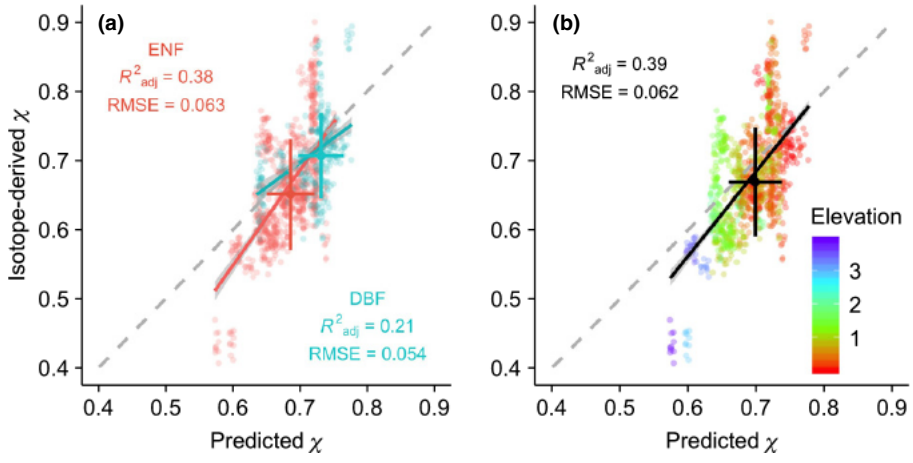

Fig. 2 Predicted vs isotope-derived 5 yr boxcar averages of χ over 1951–2014. Median and standard deviations are shown for each plant functional type (PFT) (a) or for all PFTs (b). The bold lines are the ordinary least-squares regressions for each PFT (a) or combined (b). The dashed grey line is the 1 : 1 line. DBF, deciduous broadleaf forests ($n = 29$); ENF, evergreen needleleaf forests ($n = 74$). R^2_{adj}, adjusted R^2 ($P < 0.001$); RMSE, root mean square error of the predictions. Elevation is in km.

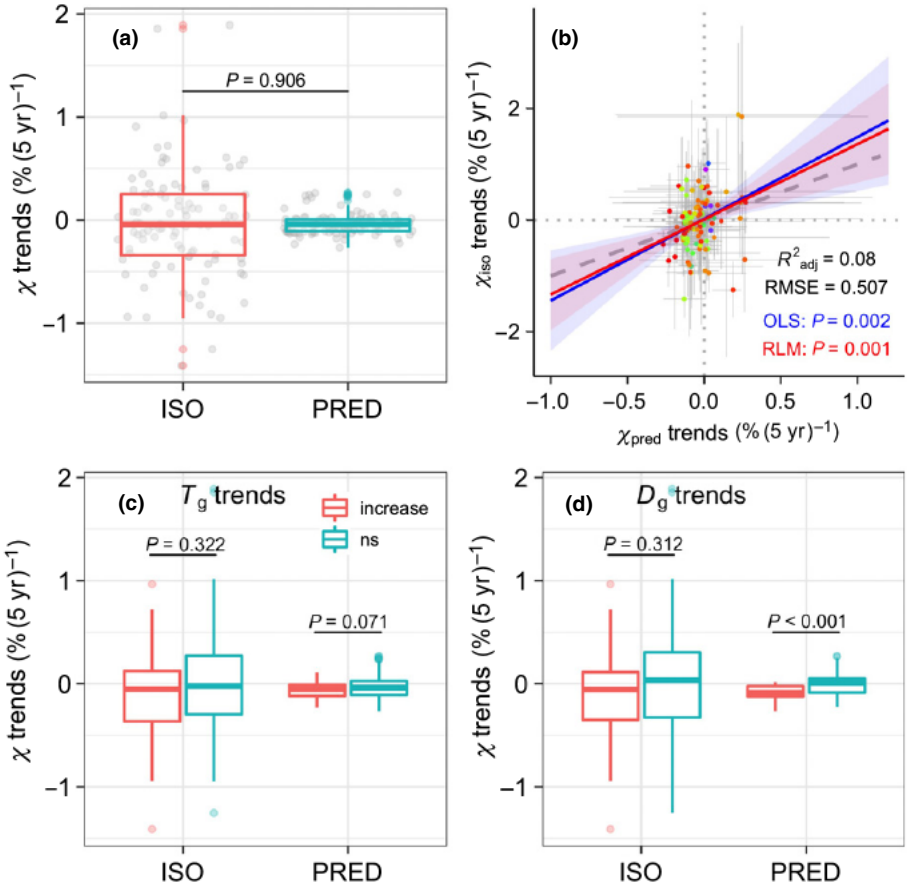

Fig. 3 Temporal changes in isotope-derived (ISO) and predicted (PRED) χ over the 1951–2014 period for the selected 103 tree-ring sites (see Supporting Information Table S1). The Theil-Sen trends of the percentage of changes relative to the site mean (% (5 yr)$^{-1}$) are presented considering all sites (a, b), or at each site depending on the historical trends in growing-season average climate variables (daytime temperature T_g (c), vapour pressure deficit D_g (d)) (ns, nonsignificant trend; increase, positive trend). In (a), (c) and (d), the *P*-values from the Student's *t*-tests performed between the different groups of trends are indicated. In (b), the 95% confidence intervals of the Theil-Sen trends are shown in light grey. The dashed grey line is the 1 : 1 line. The coloured lines with associated 95% confidence intervals are for different regression models: ordinary least squares (OLS, blue) and robust (RLM, red) linear models. The *P*-value for these models are also indicated. R^2_{adj}, adjusted R^2; RMSE, root mean square error of the predictions.

RMSE = 0.507, AIC = 159, BIC = 166), as shown using either OLS or RLM ($P < 0.003$; Fig. 3b). The relationship between χ_{iso} and χ_{pred} trends was mainly driven by ENF sites ($R^2_{adj} = 0.11$, RMSE = 0.135, AIC = −78, BIC = −73, $P = 0.003$ for ENF vs $R^2_{adj} = 0.03$, RMSE = 0.069, AIC = −67, BIC = −63, $P = 0.199$ for DBF).

Model-data comparisons against environmental drivers

The partial residuals of logit χ_{iso} values increased with increasing T_g but decreased with increasing $\log_e D_g$, c_a and z (i.e. decreasing P_{atm}), consistent with those of logit χ_{pred} (Table 1; Fig. 4). When ignoring c_a as environmental driver of χ_{iso}, the variance explained by the statistical model was similar to the one including c_a ($R^2_{adj} = 0.37$; see Table S2), the second model being only slightly improved (ANOVA, $P = 0.036$). The relatively small contribution to the explained variance of the unique effect of c_a compared with the other drivers (Table 1) suggests that c_a had only a minor effect on χ_{iso}. When significant, the logit χ_{iso} responses to changing T_g $\log_e D_g$ and c_a varied and diverged from the general pattern at some sites (Fig. 4a–c); however, no clear pattern for these discrepancies emerged.

The linear mixed-effects models for logit χ_{iso} with T_g, $\log_e D_g$, c_a and z (indexing P_{atm}) as fixed effects, and site as a random effect, performed better than the model considering only fixed effects (lower AIC and BIC, significant ANOVA test, $P < 0.001$; $R^2_{cond} = 0.94$ vs $R^2_{adj} = 0.39$; Tables 1, S2a). The model with random intercepts and slopes yielded lower AIC and BIC values than the one with only random intercepts. Both models, however, tended to assign most of the variance in logit χ_{iso} to the random effects (*c.* 64%), whereas the fixed effects only contributed *c.* 30% of the variance (Table S2a).

Model biases vs environmental constraints

Overall, the theoretical model for χ showed a significant positive bias with increasing z (decreasing P_{atm}), mainly as a result of two sites ($P < 0.001$; Fig. 5c) but no bias related to T_g, $\log_e D_g$ or c_a were detected (Figs 5a,b). Nevertheless, there were significant biases with changing T_g $\log_e D_g$ or c_a at some individual sites (Fig. 5a,b) but the magnitudes and signs of these biases varied among sites.

Including one of the indices of soil water availability (i.e. θ or α) as additional driver of logit χ_{iso} in the linear regression model slightly improved the model fits (lower AIC and BIC; significant ANOVA, $P < 0.05$) but both the dependencies of logit χ_{iso} on z and on c_a were then no longer significant (Table S2b). The model showed a significant negative bias with increasing θ and α (Fig. 6b,c), indicating an overestimation of χ at low soil moisture sites and underestimation of χ at high soil moisture sites at least over the 1979–2014 period. Note that model biases related to these additional drivers diverged from the general responses at some individual sites.

Table 1 Summary statistics for the environmental dependencies of reconstructed and predicted logit χ.

	Predictor	Estimate	SE	*t*-value	Unique	Total	R^2_{adj}	RMSE	AIC	BIC
Reconstruction	ΔT_g	0.068***	0.005	12.745	24.65	14.63	0.37***	0.306	522	552
	$\text{Log}_e D_g$	−0.520***	0.056	−9.202	12.85	6.03				
	z	−0.118***	0.026	−4.458	3.02	67.93				
	c_a	−0.009*	0.004	−2.096	0.67	36.28				
	Intercept	1.625***	0.145	10.924						
Prediction	ΔT_g	0.061***	<0.001	153.40	33.04	13.15	0.98***	0.023	−5208	−5178
	$\text{Log}_e D_g$	−0.504***	0.004	−119.95	20.20	7.08				
	z	−0.040***	0.002	−20.17	0.57	62.33				
	c_a	−0.004***	<0.001	−11.71	0.19	35.39				
	Intercept	1.401***	0.011	126.39						

ΔT_g, difference between growing-season mean temperature T_g and 25°C; $\log_e$-transformed vapour pressure deficit; $\log_e D_g$, partial pressure of CO_2 corrected for elevation effect (c_a); z, elevation; *t*-value, Student's *t*-test; 'Unique'/'Total', contributions to the explained variance (R^2) of unique effect (Unique) and both unique and common effects (Total) for each environmental driver (in % of R^2); R^2_{adj}, adjusted R^2; RMSE, root mean square error; AIC, Akaike information criterion; BIC, Bayesian information criterion. The statistical significance of the models is indicated: ***, $P < 0.001$; *, $P < 0.05$.

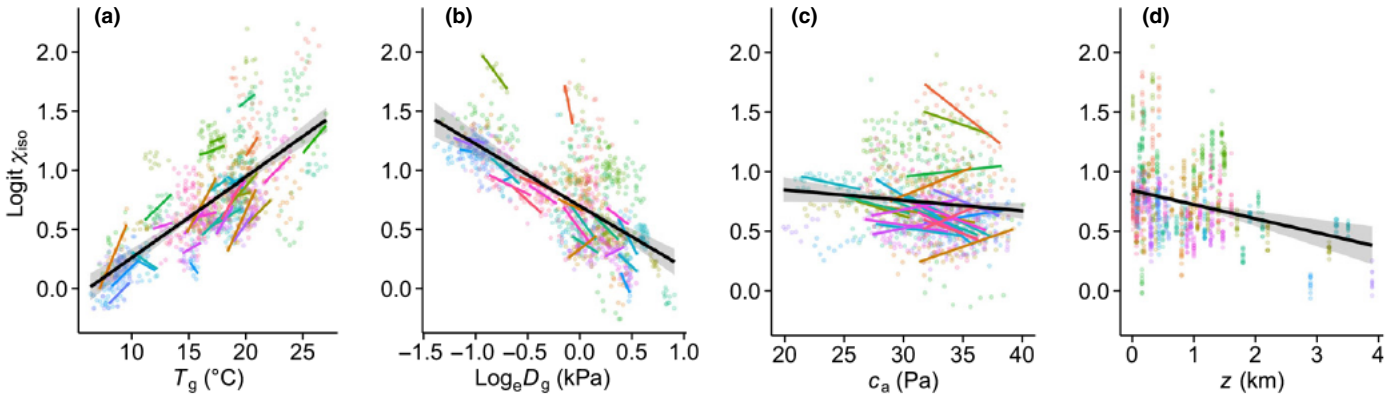

Fig. 4 Partial residual plots showing temporal and spatial variations in the 5 yr boxcar average of logit χ derived from tree-ring stable carbon isotope data as a function of growing-season average climate variables (daytime temperature T_g (a), $\log_e$-transformed vapour pressure deficit D_g (b)), partial pressure of CO_2 (c_a) corrected for elevation effect (c) and elevation (z) indexing P_{atm} (d) over 1951–2014. The different colours correspond to different sites. The solid colour lines indicate the modelled response from the multiple linear regression models for each site, and the solid black lines are those for all sites combined (see Table 1 for statistics). The grey shaded area represents the 95% confidence interval of the regression. Only significant trends at 95% ($P < 0.05$) are shown.

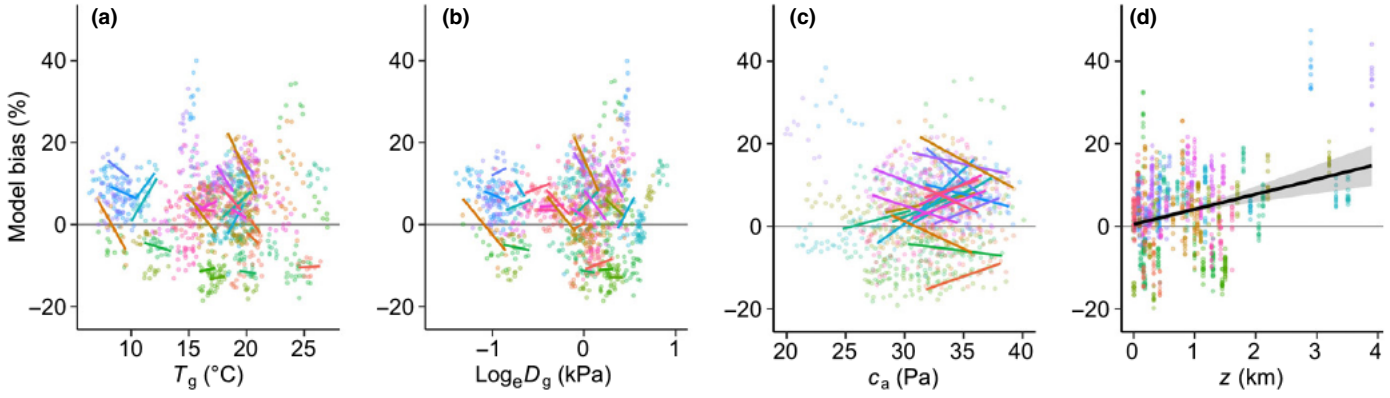

Fig. 5 Partial residual of the model bias (%) in χ predicted by the theoretical model plotted against growing-season mean daytime climate variables (temperature T_g (a), $\log_e$-transformed vapour pressure deficit D_g (b)), partial pressure of CO_2 (c_a) corrected for elevation effect (c) and elevation z (d) over 1951–2014. The different colours correspond to different sites. The solid colour lines indicate the modelled response from the multiple linear regression models for each site, and the solid black lines are those for all sites combined. The grey-shaded area represents the 95% confidence interval for the regression line. Only significant regression lines ($P < 0.05$) are shown.

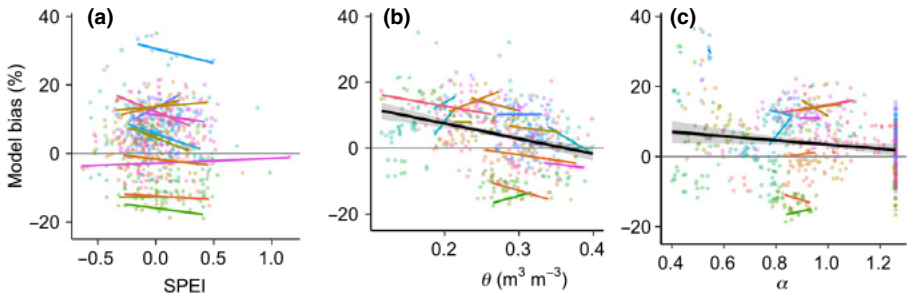

Fig. 6 Partial residual plots of the model bias (%) in χ predicted by the theoretical model plotted against growing-season average water availability or drought indices over 1979–2014: (a) Standardized Precipitation-Evapotranspiration Index, SPEI; (b) surface soil moisture content, θ; (c) Priestley–Taylor coefficient, α (see Supporting Information Table S2b). The different colours correspond to different sites. The solid colour lines indicate the modelled response from the multiple linear regression models for each site, and the solid black lines are those for all sites combined. The grey-shaded area represents the 95% confidence interval for the regression line. Only significant trends at 95% ($P < 0.05$) are shown.

Discussion

The aim of our study was to evaluate long-term values and trends of χ as predicted by the least-cost hypothesis against a large network of stable C isotope-derived χ series from tree rings. Our results are compelling, as they demonstrate that despite uncertainties related to the use of tree-ring $\delta^{13}C$ data as proxy of leaf-gas exchanges (see also Notes S4), the model predicted 39% of the variance in χ across sites and years. However, only 8% of the variance in χ trends across years was explained by the model, in part because of the larger site-to-site variability in χ trends reported in the tree-ring dataset compared with the predictions. In the following sections, we address both the skills and limitations of the model for predicting plant stomatal and photosynthetic adjustments to environmental conditions. We also discuss potential additional drivers of χ to consider in future studies.

Main drivers influencing χ and biases in the model

Rising T_g increases photosynthetic costs by increasing the Michaelis constant of Rubisco (K), while reducing water transport costs as a result of the reduced viscosity of water (η^*). Both effects combined with the increase in the photorespiratory compensation point (Γ^*) with higher T_g are expected to lead to higher ξ (Eqn 4). However, D_g tends to increase with rising T_g, so the effect of temperature on χ, being influenced in opposite ways by ξ and D_g (Wang *et al.*, 2017a), is not straightforward to predict. Increasing D_g tends to increase the water transport required per mole of C fixed, and thus the transpiration costs, leading to lower χ. Decreasing P_{atm} decreases K, as a result of the reduced partial pressure of O_2, thereby increasing the affinity of Rubisco for CO_2 and reducing the carboxylation capacity required per mole of C fixed. At the same time (all else being equal) the actual vapour pressure declines while the saturated vapour pressure remains constant, implying an increase in D_g. Thus, as P_{atm} decreases (z increases), both effects preferentially enhance Rubisco capacity relative to water transport capacity, favouring a lower χ (Körner & Diemer, 1987; Körner *et al.*, 1991; Terashima *et al.*, 1995; Wang *et al.*, 2017a). Finally, elevated c_a increases photosynthesis by increasing the carboxylation rate, while also increasing the transpiration efficiency of plants via a decrease in stomatal conductance. As a result, the direct effect of c_a on χ is difficult to assess at first glance.

In general, rising T_g tended to cause an increase of logit χ_{iso}, suggesting that the temperature dependencies of K, Γ^* and η^* had a stronger impact on χ than that of D_g (Fig. 5a). As expected, lower χ_{iso} values were observed with increasing D_g and z (Fig. 5b, c), consistent with previous studies (Körner & Diemer, 1987; Körner *et al.*, 1991; Zhu *et al.*, 2010). Overall, the slight decrease in logit χ_{iso} with rising c_a implies that c_i increases less than proportionally to an increase in c_a. The stronger unique effects of T_g and D_g relative to P_{atm} and c_a on logit χ_{iso} (Table 1) suggests that both T_g and D_g are the dominant drivers of change in χ at many sites. The apparently divergent responses (relative to the general pattern) of logit χ_{iso} to T_g, D_g and c_a at some sites may be indicative of site-specific characteristics not included in the model that also contributed to changes in χ_{iso}. It is also plausible that both T_g and D_g data inferred from the 0.5° resolution CRU dataset, or even the c_a data mainly derived from the Mauna Loa Observatory (Hawaii), were not fully capturing microclimatic differences between or within sites.

The environmental dependencies of χ were, for the most part, captured correctly by the theoretical model (Table 1). Nonetheless, the model tended to underestimate the negative impact of decreasing P_{atm} (increasing z) on χ values (Table 1; Fig. 6c), suggesting that the observational data were more sensitive to lower P_{atm} (higher z) than predicted by the theory. The positive bias in predicted χ at high-elevation sites was mainly a result of two ENF sites, both located in the mountains of Kashmir (Table S1; Treydte *et al.*, 2009), and thus could also be an artefact of site selection. These sites were characterised by the lowest mean T_g and D_g values and wettest conditions in the network for the sites located at altitudes > 2.5 km. It is thus plausible that the combined effects of relatively low T_g and low D_g on χ have dampened the negative effect of low P_{atm} (high z) on predicted χ values. It is worth noting that the dependency of χ on z depends on the relative humidity and the actual vapour pressure. As a result, the predicted coefficient for the elevational dependency of χ in the linear regression (here −0.040; Table 1) is not expected to be of the same magnitude as the theoretical coefficient estimated under standard conditions (T = 25°C, relative humidity = 50%) in the former study (i.e. Wang *et al.*, 2017b: −0.0815; see Notes S5).

Other potential controls on χ

The large variability in the magnitude of χ_{iso} trends among sites (Fig. 3) and the different dependences of χ_{iso} to the environmental constraints at some sites (Fig. 5) suggest that other controls on χ not captured by the model are operating and may explain part of the remaining variance in χ_{iso} that was mostly assigned to random effects by the linear mixed-effects models (Table S2a). For instance, the least-cost hypothesis considers the influence of atmospheric demand for water on χ but does not predict how dry soils further influence χ (Verhoef & Egea, 2014; Rogers *et al.*, 2017). Here we found that, independent of the individual effects of T_g, D_g, c_a and z on χ, the model tended to underestimate χ values at high soil moisture and to overestimate χ values at low soil moisture (Fig. 7b,c). In a meta-analysis of drying experiments, Zhou *et al.* (2013) demonstrated that the parameter g_1 of the Medlyn *et al.* (2011) model, based on the Cowan–Farquhar optimality hypothesis (mathematically equivalent to ξ in the least-cost model) is reduced by low soil moisture, and that this occurs at a less negative predawn water potential than the decline in V_{cmax} that occurs in very dry soils. Thus, under drying conditions with reduced soil water availability, χ is expected to decrease via a reduction of ξ. Nonetheless, because D_g and soil moisture are tightly coupled at weekly to monthly timescales (Sulman *et al.*, 2016; Gentine *et al.*, 2019), their relative contributions on changes in χ may be difficult to disentangle (Buckley, 2017; Zhou *et al.*, 2019; Yi *et al.*, 2019), complicating the inclusion of soil water limitation in the framework of the least-cost optimality hypothesis. Recent research testing empirical parameterizations of the effect of soil moisture on gross primary production suggests that the value for β, held constant here, should in fact decline with decreasing soil moisture content (Stocker *et al.*, 2018, 2019b). Further research at sites with different soil water availability and different evaporative demand should help in implementing soil moisture effect in the model through a theoretically motivated reduction of β.

Some studies have suggested that increases in leaf N content with fossil fuel combustion and agricultural emissions (Galloway *et al.*, 2008) might stimulate photosynthetic capacity (Walker *et al.*, 2014) and increase stomatal conductance, resulting in changes in $\Delta^{13}C$ and χ. Based on experiments where N and S fertilizers were applied directly to tree canopies, Guerrieri *et al.* (2011) found strong effects of both on $\Delta^{13}C$ and χ, with the magnitude of changes related to the element and the time since application or cessation. Their results generally agreed with previous work demonstrating that the effect of N fertilization on tree-ring $\Delta^{13}C$ is short-lived (Brooks & Coulombe, 2009). Nevertheless, the causal mechanisms underlying $\Delta^{13}C$ responses to both climate and N deposition are not well established (Leonardi *et al.*, 2012). Based on an observational global dataset of V_{cmax}, Smith *et al.* (2019) showed that the dependence of V_{cmax} on leaf N was overestimated in vegetation models, as also suggested by Rogers (2014) – and that V_{cmax} can be predicted accurately from T_g, D_g, z and light availability alone. These findings suggest that leaf N deposition is not a primary driver of photosynthetic capacity, but rather that the photosynthetic demand itself constrains leaf N content (Dong *et al.*, 2017). Thus, even though changes in leaf N concentrations accompanying changes in V_{cmax} can affect both $\Delta^{13}C$ and χ, we suggest that the environmental drivers of such variations are implicitly included in the least-cost optimality model.

Even though some processes influencing χ may be missing, our compilation of 103 tree-ring $\Delta^{13}C$ records supports the theoretical optimal responses of χ to a combination of T_g, D_g, P_{atm} and c_a over the period 1951–2014 as predicted by the least-cost hypothesis (Prentice *et al.*, 2014; Wang *et al.*, 2017b). Crucially, the theory predicts χ to be only slightly dependent on c_a, implying that rising c_a leads to a quasi-proportional increase in c_i and an increase in the biochemical rate of C uptake (Farquhar *et al.*, 1980). As c_a rises, the ratio of Γ^* to c_a declines and the average responses of χ to c_a converges to zero (Eqn 4). This response is supported by experimental studies showing no change or a small decrease in χ, on average, with sustained CO_2 enrichment (Ainsworth & Long, 2005) and by historical studies (Keeling *et al.*, 2017; Schubert & Jahren, 2018). This response, however, also contrasts with several studies using leaf and wood $\delta^{13}C$ measurements from CO_2 enrichment experiments and/or palaeorecords apparently showing an increase of χ with rising c_a at c_a values ranging from 200 to 600 ppm (Voelker *et al.*, 2016; Hare *et al.*, 2018), or even a large decrease of χ with sustained CO_2 enrichment (Battipaglia *et al.*, 2013). It is worth noting that these studies did not include the photorespiration term in the discrimination model. The apparently strong influence of rising c_a on χ in these studies might be an artefact caused by disregarding this effect, as was also indicated by Schubert & Jahren (2018) and Lavergne *et al.* (2019). Our analysis of partial residuals of logit χ_{iso} suggests that, across geographically and phylogenetically diverse trees, the average response of χ_{iso} to c_a is weak (Table 1; Fig. 5), as predicted by the least-cost hypothesis.

Our results have strong implications for the understanding of the coupled terrestrial C and water cycles, because they indicate that the increase in iWUE expected with rising atmospheric CO_2 can be offset by increasing T_g (or, potentially, by decreasing D_g and/or increasing soil moisture availability). Also, for the same increase in atmospheric CO_2, iWUE may increase with decreasing P_{atm} (increasing z). Our research complements recent attempts to quantify the relative contributions of environmental drivers to changes in plant water use (Frank *et al.*, 2015; Dekker *et al.*, 2016; Adams *et al.*, 2019) by highlighting eco-evolutionary optimality mechanisms underlying these changes.

Current vegetation and land-surface models suffer from large uncertainties, mainly as a result of incomplete or inaccurate representations of the fundamental processes governing not only leaf-level gas exchange (Raczka *et al.*, 2018), but also competition, C allocation, demography and responses to disturbances such as wildfires and insect attacks. Improving the representation of ecophysiological responses to the environment is only part of a much bigger problem with current terrestrial models. It is a central part, nonetheless, and our research suggests a way forward – based on optimality theory – for the representation of the coupled terrestrial C and water cycles in next-generation Earth system models.

Acknowledgements

We thank the three anonymous reviewers for their useful and constructive comments and suggestions. We acknowledge all data providers and the many contributors who helped produce the dataset analysed here. AL was supported by a Postdoctoral Newton International Fellowship (grant no. NF170082) funded by the Royal Society (UK). ID-L received financial support from Fundació La Caixa through the Junior Leader Program (LCF/BQ/LR18/11640004). This work contributes to the AXA Chair Programme in Biosphere and Climate Impacts and the Imperial College initiative on Grand Challenges in Ecosystems and the Environment. The project has also received funding from the European Research Council (ERC) under the European Union's Horizon 2020 Research and Innovation Programme (grant agreement no: 787203 REALM).

Author contributions

AL and ICP designed the research. HG provided additional suggestions on the research plans. SV, AC, HJdeB, VD, IR, ID-L, EM-S, GB, FCM, JJC, RC, YF, AM, CJS, RMK, JSR and TED provided tree-ring C isotopic data. AL compiled and analysed the data. AL and KJB computed the linear mixed-effect models. AL wrote the paper with inputs and revisions from all co-authors.

ORCID

Giovanna Battipaglia https://orcid.org/0000-0003-1741-3509
J. Julio Camarero https://orcid.org/0000-0003-2436-2922
Adam Csank https://orcid.org/0000-0002-7001-4470
Valérie Daux https://orcid.org/0000-0002-8643-260X
Isabel Dorado-Liñán https://orcid.org/0000-0002-8913-0420
Heather Graven https://orcid.org/0000-0003-3934-2502
Aliénor Lavergne https://orcid.org/0000-0002-4591-1217
Elisabet Martínez-Sancho https://orcid.org/0000-0003-4413-6818
Annette Menzel https://orcid.org/0000-0002-7175-2512
Iain Robertson https://orcid.org/0000-0001-7174-4523
Steve Voelker https://orcid.org/0000-0002-0110-3381

References

Adams MA, Buckley TN, Turnbull TL. 2019. Rainfall drives variation in rates of change in intrinsic water use efficiency of tropical forests. *Nature Communications* **10**: 1–8.

Ainsworth EA, Long SP. 2005. What have we learned from 15 years of free-air CO_2 enrichment (FACE)? A meta-analytic review of the responses of photosynthesis, canopy properties and plant production to rising CO_2. *New Phytologist* **165**: 351–372.

Akaike H. 1973. Information theory and an extension of the maximum likehood principle. In: Second International Symposium on Information Theory. 267–281.

Allen RG, Pereira LS, Raes D, Smith M. 1998. Crop evapotranspiration - Guidelines for computing crop water requirements – FAO Irrigation and drainage paper 56. *Irrigation and Drainage* 1–15.

Badeck FW, Tcherkez G, Nogués S, Piel C, Ghashghaie J. 2005. Post-photosynthetic fractionation of stable carbon isotopes between plant organs – a widespread phenomenon. *Rapid Communications in Mass Spectrometry* **19**: 1381–1391.

Ballantyne AP, Andres R, Houghton R, Stocker BD, Wanninkhof R, Anderegg W, Cooper LA, DeGrandpre M, Tans PP, Miller JB *et al.* 2015. Audit of the global carbon budget: Estimate errors and their impact on uptake uncertainty. *Biogeosciences* **12**: 2565–2584.

Ballantyne AP, Miller JB, Tans PP. 2010. Apparent seasonal cycle in isotopic discrimination of carbon in the atmosphere and biosphere due to vapor pressure deficit. *Global Biogeochemical Cycles* **24**: 1–16.

Bates D, Mächler M, Bolker B, Walker S. 2015. Fitting linear mixed-effects models using lme4. *Journal of Statistical Software* **67**: 1–48.

Battipaglia G, Saurer M, Cherubini P, Calfapietra C, Mccarthy HR, Norby RJ, Francesca Cotrufo M. 2013. Elevated CO_2 increases tree-level intrinsic water use efficiency: Insights from carbon and oxygen isotope analyses in tree rings across three forest FACE sites. *New Phytologist* **197**: 544–554.

Beguería S, Vicente-Serrano SM, Angulo-Martínez M. 2010. A multiscalar global drought dataset: The SPEI base: a new gridded product for the analysis of drought variability and impacts. *Bulletin of the American Meteorological Society* **91**: 1351–1356.

Bernacchi CJ, Singsaas EL, Pimentel C, Portis AR Jr, Long SP. 2001. Improved temperature response functions for models of Rubisco-limited photosynthesis. *Plant, Cell & Environment* **24**: 253–259.

Bloomfield KJ, Prentice IC, Cernusak LA, Eamus D, Medlyn BE, Wright IJ, Boer MM, Cale P, Cleverly J, Egerton JJG *et al.* 2019. The validity of optimal leaf traits modelled on environmental conditions. *New Phytologist* **221**: 1409–1423.

Bolker BM, Brooks ME, Clark CJ, Geange SW, Poulsen JR, Stevens MHH, White JSS. 2009. Generalized linear mixed models: a practical guide for ecology and evolution. *Trends in Ecology and Evolution* **24**: 127–135.

Bowling DR, Pataki DE, Randerson JT. 2008. Carbon isotopes in terrestrial ecosystem pools and CO_2 fluxes. *New Phytologist* **178**: 24–40.

Brooks JR, Coulombe R. 2009. Physiological responses to fertilization recorded in tree rings: isotopic lessons from a long-term fertilization trial. *Ecological Applications* **19**: 1044–1060.

Buckley TN. 2017. Modeling stomatal conductance. *Plant Physiology* **174**: 572–582.

Buckley TN, Schymanski SJ. 2014. Stomatal optimisation in relation to atmospheric CO_2. *New Phytologist* **201**: 372–377.

von Caemmerer S, Evans JR. 2015. Temperature responses of mesophyll conductance differ greatly between species. *Plant, Cell & Environment* **38**: 629–637.

Ciais P, Sabine C, Bala G, Bopp L, Brovkin V, Canadell J, Chhabra A, DeFries R, Galloway J, Heimann M *et al.* 2013. 2013: Carbon and other biogeochemical cycles. Climate Change 2013: The Physical Science Basis. Contribution of Working Group I to the Fifth Assessment Report of the Intergovernmental Panel on Climate Change: 465–570.

Cowan IR, Farquhar GD. 1977. Stomatal function in relation to leaf metabolism and environment. *Symposia of the Society for Experimental Biology* **31**: 471–505.

Craig H. 1953. The geochemistry of the stable carbon isotopes. *Geochimica et Cosmochimica Acta* **3**: 53–92.

Davis TW, Prentice IC, Stocker BD, Thomas RT, Whitley RJ, Wang H, Evans BJ, Gallego-Sala AV, Sykes MT, Cramer W. 2017. Simple process-led algorithms for simulating habitats (SPLASH vol 1.0): Robust indices of radiation, evapotranspiration and plant-available moisture. *Geoscientific Model Development* **10**: 689–708.

Dekker SC, Groenendijk M, Booth BBB, Huntingford C, Cox PM. 2016. Spatial and temporal variations in plant water-use efficiency inferred from tree-ring, eddy covariance and atmospheric observations. *Earth System Dynamics* **7**: 525–533.

Dewar R, Mauranen A, Mäkelä A, Hölttä T, Medlyn B, Vesala T. 2018. New insights into the covariation of stomatal, mesophyll and hydraulic conductances from optimization models incorporating nonstomatal limitations to photosynthesis. *New Phytologist* **217**: 571–585.

Dong N, Prentice IC, Evans BJ, Caddy-Retalic S, Lowe AJ, Wright IJ. 2017. Leaf nitrogen from first principles: field evidence for adaptive variation with climate. *Biogeosciences* **14**: 481–495.

Dorado-Liñán I, Piovesan G, Martínez-Sancho E, Gea-Izquierdo G, Zang C, Cañellas I, Castagneri D, Di Filippo A, Gutiérrez E, Ewald J *et al.* 2019. Geographical adaptation prevails over species-specific determinism in trees' vulnerability to climate change at Mediterranean rear-edge forests. *Global Change Biology* **25**: 1296–1314.

Dorigo W, Wagner W, Albergel C, Albrecht F, Balsamo G, Brocca L, Chung D, Ertl M, Forkel M, Gruber A *et al.* 2017. ESA CCI Soil Moisture for improved Earth system understanding: state-of-the art and future directions. *Remote Sensing of Environment* **203**: 185–215.

Ehleringer JR, Hall AE, Farquhar GD. 1993. Water use in relation to productivity. In: Ehleringer JR, Hall A, Farquhar GD, eds. *Stable isotopes and plant carbon-water relations*. San Diego, CA, USA: Academic Press, 155–172.

Evans JR, Von Caemmerer S. 2013. Temperature response of carbon isotope discrimination and mesophyll conductance in tobacco. *Plant, Cell & Environment* **36**: 745–756.

Eyring V, Bony S, Meehl GA, Senior C, Stevens B, Stouffer RJ, Taylor KE. 2016. Overview of the Coupled Model Intercomparison Project Phase 6 (CMIP6) experimental design and organisation. *Geoscientific Model Development Discussions* **8**: 10539–10583.

Farquhar GD, von Caemmerer S, Berry JA. 1980. A biochemical model of photosynthetic CO_2 assimilation in leaves of C_3 species. *Planta* **149**: 78–90.

Farquhar GD, O'Leary MH, Berry JA. 1982. On the relationship between carbon isotope discrimination and the intercellular carbon dioxide concentration in leaves. *Australian Journal of Plant Physiology* **9**: 121–137.

Flexas J, Ribas-Carbó M, Diaz-Espejo A, Galmés J, Medrano H. 2008. Mesophyll conductance to CO_2: Current knowledge and future prospects. *Plant, Cell & Environment* **31**: 602–621.

Fox J, Weisberg S. 2018. Visualizing fit and lack of fit in complex regression models with predictor effect plots and partial residuals. *Journal of Statistical Software* **87**: 1–27.

Frank DC, Poulter B, Saurer M, Esper J, Huntingford C, Helle G, Treydte K, Zimmermann NE, Schleser GH, Ahlström A *et al.* 2015. Water-use efficiency and transpiration across European forests during the Anthropocene. *Nature Climate Change* **5**: 579–583.

Fürstenau Togashi H, Colin Prentice I, Atkin OK, Macfarlane C, Prober SM, Bloomfield KJ, Evans BJ. 2018. Thermal acclimation of leaf photosynthetic traits in an evergreen woodland, consistent with the coordination hypothesis. *Biogeosciences* **15**: 3461–3474.

Galloway JN, Townsend AR, Erisman JW, Bekunda M, Cai Z, Freney JR, Martinelli LA, Seitzinger SP, Sutton MA. 2008. Transformation of the nitrogen cycle: recent trends, questions, and potential solutions. *Science* **320**: 889–892.

Gentine P, Green J, Guerin M, Humphrey V, Seneviratne SI, Zhang Y, Zhou S. 2019. Coupling between the terrestrial carbon and water cycles – a review. *Environmental Research Letters* **14**, 1–18.

Gessler A, Ferrio JP, Hommel R, Treydte K, Werner RA, Monson RK. 2014. Stable isotopes in tree rings: towards a mechanistic understanding of isotope fractionation and mixing processes from the leaves to the wood. *Tree Physiology* **34**: 796–818.

Ghashghaie J, Badeck F-W, Lanigan G, Nogués S, Tcherkez G, Deléens E, Cornic G, Griffiths H. 2003. Carbon isotope fractionation during dark respiration and photorespiration in C_3 plants. *Phytochemistry Reviews* **2**: 145–161.

Gimeno TE, Saavedra N, Ogée J, Medlyn BE, Wingate L. 2019. A novel optimization approach incorporating non-stomatal limitations predicts stomatal behaviour in species from six plant functional types. *Journal of Experimental Botany* **70**: 1639–1651.

Givnish TJ. 1986. Optimal stomatal conductance, allocation of energy between leaves and roots, and the marginal cost of transpiration. In: Givnish TJ, ed. *On the economy of plant form and function*. Cambridge, UK: Cambridge University Press, 171–213.

Graven H, Allison CE, Etheridge DM, Hammer S, Keeling RF, Levin I, Meijer HAJ, Rubino M, Tans PP, Trudinger CM *et al.* 2017. Compiled records of carbon isotopes in atmospheric CO_2 for historical simulations in CMIP6. *Geoscientific Model Development* **10**: 4405–4417.

Green JK, Seneviratne SI, Berg AM, Findell KL, Hagemann S, Lawrence DM, Gentine P. 2019. Large influence of soil moisture on long-term terrestrial carbon uptake. *Nature* **565**: 476–479.

Guerrieri R, Mencuccini M, Sheppard LJ, Saurer M, Perks MP, Levy P, Sutton MA, Borghetti M, Grace J. 2011. The legacy of enhanced N and S deposition as revealed by the combined analysis of $\Delta^{13}C$, $\Delta^{18}O$ and $\Delta^{15}N$ in tree rings. *Global Change Biology* **17**: 1946–1962.

Hare VJ, Loftus E, Jeffrey A, Ramsey CB. 2018. Atmospheric CO_2 effect on stable carbon isotope composition of terrestrial fossil archives. *Nature Communications* **9**: 252.

Harris I, Jones PD, Osborn TJ, Lister DH. 2014. Updated high-resolution grids of monthly climatic observations – the CRU TS3.10 Dataset. *International Journal of Climatology* **34**: 623–642.

Huber ML, Perkins RA, Laesecke A, Friend DG, Sengers JV, Assael MJ, Metaxa IN, Vogel E, Mares R, Miyagawa K. 2009. New international formulation for the viscosity of H_2O. *Journal of Physical and Chemical Reference Data* **38**: 101–125.

Humphrey V, Zscheischler J, Ciais P, Gudmundsson L, Sitch S, Seneviratne SI. 2018. Sensitivity of atmospheric CO_2 growth rate to observed changes in terrestrial water storage. *Nature* **560**: 628–631.

Jones HG. 2013. *Plants and microclimate*. Cambridge, UK: Cambridge University Press.

Jones CD, Arora V, Friedlingstein P, Bopp L, Brovkin V, Dunne J, Graven H, Hoffman F, Ilyina T, John JG *et al.* 2016. C4MIP-the coupled climate-carbon cycle model intercomparison project: experimental protocol for CMIP6. *Geoscientific Model Development* **9**: 2853–2880.

Katul G, Manzoni S, Palmroth S, Oren R. 2010. A stomatal optimization theory to describe the effects of atmospheric CO_2 on leaf photosynthesis and transpiration. *Annals of Botany* **105**: 431–442.

De Kauwe MG, Medlyn BE, Zaehle S, Walker AP, Dietze MC, Hickler T, Jain AK, Luo Y, Parton WJ, Prentice IC *et al.* 2013. Forest water use and water use efficiency at elevated CO_2: a model-data intercomparison at two contrasting temperate forest FACE sites. *Global Change Biology* **19**: 1759–1779.

De Kauwe MG, Medlyn BE, Zaehle S, Walker AP, Dietze MC, Wang Y-P, Luo Y, Jain AK, El-Masri B, Hickler T *et al.* 2014. Where does the carbon go? A model-data intercomparison of vegetation carbon allocation and turnover processes at two temperate forest free-air CO_2 enrichment sites. *New Phytologist* **203**: 883–899.

Keeling RF, Graven HD, Welp LR, Resplandy L, Bi J, Piper SC, Sun Y, Bollenbacher A, Meijer HAJ. 2017. Atmospheric evidence for a global secular increase in carbon isotopic discrimination of land photosynthesis. *Proceedings of the National Academy of Sciences, USA* **114**: 10361–10366.

Keller KM, Lienert S, Bozbiyik A, Stocker TF, Churakova Sidorova OV, Frank DC, Klesse S, Koven CD, Leuenberger M, Riley WJ *et al.* 2017. 20th century changes in carbon isotopes and water-use efficiency: Tree-ring-based evaluation of the CLM4.5 and LPX-Bern models. *Biogeosciences* **14**: 2641–2673.

Knorr W, Prentice IC, House JI, Holland EA. 2005. Long-term sensitivity of soil carbon turnover to warming. *Nature* **433**: 298–301.

Körner C, Diemer M. 1987. In situ photosynthetic responses to light, temperature and carbon dioxide in herbaceous plants from low and high altitude. *Functional Ecology* **1**: 179–194.

Körner C, Farquhar GD, Wong SC. 1991. Carbon isotope discrimination by plants follows latitudinal and altitudinal trends. *Oecologia* **88**: 30–40.

Lavergne A, Graven H, De Kauwe MG, Keenan TF, Medlyn BE, Prentice IC. 2019. Observed and modelled historical trends in the water-use efficiency of plants and ecosystems. *Global Change Biology* **25**: 2242–2257.

Leonardi S, Gentilesca T, Guerrieri R, Ripullone F, Magnani F, Mencuccini M, Noije TV, Borghetti M. 2012. Assessing the effects of nitrogen deposition and climate on carbon isotope discrimination and intrinsic water-use efficiency of angiosperm and conifer trees under rising CO_2 conditions. *Global Change Biology* **18**: 2925–2944.

Li J, Wang G, Mayes MA, Allison SD, Frey SD, Shi Z, Hu X-M, Luo Y, Melillo JM. 2018. Reduced carbon use efficiency and increased microbial turnover with soil warming. *Global Change Biology* **25**: 900–910.

Lüdecke D, Makowski D, Waggoner P. 2019. *performance: Assessment of regression models performance. R package v.0.2.0.9000.* [WWW document] URL https://easystats.github.io/performance/.

Manzoni S, Vico G, Palmroth S, Porporato A, Katul G. 2013. Optimization of stomatal conductance for maximum carbon gain under dynamic soil moisture. *Advances in Water Resources* **62**: 90–105.

Martínez-Sancho E, Dorado-Liñán I, Gutiérrez Merino E, Matiu M, Helle G, Heinrich I, Menzel A. 2018. Increased water-use efficiency translates into contrasting growth patterns of Scots pine and sessile oak at their southern distribution limits. *Global Change Biology* **24**: 1012–1028.

Medlyn BE, Duursma RA, De Kauwe MG, Prentice IC. 2013. The optimal stomatal response to atmospheric CO_2 concentration: Alternative solutions, alternative interpretations. *Agricultural and Forest Meteorology* **182–183**: 200–203.

Medlyn BE, Duursma RA, Eamus D, Ellsworth DS, Prentice IC, Barton CVM, Crous KY, De Angelis P, Freeman M, Wingate L. 2011. Reconciling the optimal and empirical approaches to modelling stomatal conductance. *Global Change Biology* **17**: 2134–2144.

Moldover MR, Trusler JPM, Edwards TJ, Mehl JB, Davis RS. 1988. Measurement of the universal gas constant R using a spherical acoustic resonator. *Journal of Research of the National Bureau of Standards* **93**: 85–114.

Nimon K, Oswald F, Roberts JK. 2013. *yhat: Interpreting Regression Effects. R package v.2.0-0.* [WWW document] URL https://CRAN.R-project.org/package=yhat.

Park R, Epstein S. 1960. Carbon isotope fractionation during photosynthesis. *Geochimica et Cosmochimica Acta* **21**: 110–226.

Peters W, van der Velde IR, van Schaik E, Miller JB, Ciais P, Duarte HF, van der Laan-Luijkx IT, van der Molen MK, Scholze M, Schaefer K *et al.* 2018. Increased water-use efficiency and reduced CO_2 uptake by plants during droughts at a continental scale. *Nature Geoscience* **11**: 744–748.

Pohlert T. 2018. *trend: Non-parametric trend tests and change-point detection. R package v.1.1.1.* [WWW document] URL https://CRAN.R-project.org/package=trend.

Prentice IC, Dong N, Gleason SM, Maire V, Wright IJ. 2014. Balancing the costs of carbon gain and water transport: Testing a new theoretical framework for plant functional ecology. *Ecology Letters* **17**: 82–91.

Le Quéré C, Andrew RM, Friedlingstein P, Sitch S, Hauck J, Pongratz J, Pickers PA, Korsbakken JI, Peters GP, Canadell JG *et al.* 2018. Global carbon budget 2018. *Earth System Science Data* **10**: 2141–2194.

R Core Team, R Development Core Team. 2018. R: A language and environment for statistical computing. (RDC Team, Ed.). *R Foundation for Statistical Computing* **1**: 409.

Raczka B, Dietze MC, Serbin SP, Davis KJ. 2018. What limits predictive certainty of long-term carbon uptake? *Journal of Geophysical Research: Biogeosciences* **123**: 3570–3588.

Raczka B, Duarte HF, Koven CD, Ricciuto D, Thornton PE, Lin JC, Bowling DR. 2016. An observational constraint on stomatal function in forests: Evaluating coupled carbon and water vapor exchange with carbon isotopes in the Community Land Model (CLM4.5). *Biogeosciences* **13**: 5183–5204.

Reich PB, Hobbie SE. 2013. Decade-long soil nitrogen constraint on the CO_2 fertilization of plant biomass. *Nature Climate Change* **3**: 278–282.

Reich PB, Hobbie SE, Lee T, Ellsworth DS, West JB, Tilman D, Knops JMH, Naeem S, Trost J. 2006. Nitrogen limitation constrains sustainability of ecosystem response to CO_2. *Nature* **440**: 922–925.

Rogers A. 2014. The use and misuse of $V_{c,\,max}$ in Earth System Models. *Photosynthesis Research* **119**: 15–29.

Rogers A, Medlyn BE, Dukes JS, Bonan G, von Caemmerer S, Dietze MC, Kattge J, Leakey ADB, Mercado LM, Niinemets Ü *et al.* 2017. A roadmap for improving the representation of photosynthesis in Earth system models. *New Phytologist* **213**: 22–42.

Saurer M, Spahni R, Frank DC, Joos F, Leuenberger M, Loader NJ, McCarroll D, Gagen M, Poulter B, Siegwolf RTW *et al.* 2014. Spatial variability and temporal trends in water-use efficiency of European forests. *Global Change Biology* **20**: 3700–3712.

Schimel D, Stephens BB, Fisher JB. 2015. Effect of increasing CO_2 on the terrestrial carbon cycle. *Proceedings of the National Academy of Sciences, USA* **112**: 436–441.

Schubert BA, Jahren AH. 2018. Incorporating the effects of photorespiration into terrestrial paleoclimate reconstruction. *Earth-Science Reviews* **177**: 637–642.

Seibt U, Rajabi A, Griffiths H, Berry JA. 2008. Carbon isotopes and water use efficiency: Sense and sensitivity. *Oecologia* **155**: 441–454.

Sen PK. 1968. Estimates of the regression coefficient based on Kendall's tau. *Journal of the American Statistical Association* **63**: 1379–1389.

Smith NG, Keenan TF, Colin Prentice I, Wang H, Wright IJ, Niinemets Ü, Crous KY, Domingues TF, Guerrieri R, Yoko Ishida F *et al.* 2019. Global photosynthetic capacity is optimized to the environment (S Niu, Ed.). *Ecology Letters* **22**: 506–517.

Sperry JS, Venturas MD, Anderegg WRL, Mencuccini M, Mackay DS, Wang Y, Love DM. 2017. Predicting stomatal responses to the environment from the optimization of photosynthetic gain and hydraulic cost. *Plant, Cell & Environment* **40**: 816–830.

Stocker BD, Wang H, Smith NG, Harrison SP, Keenan TF, Sandoval D, Davis T, Prentice IC. 2019a. P-model v1.0: An optimality-based light use efficiency model for simulating ecosystem gross primary production. *Geoscientific Model Development Discussions* **37**: 1–59.

Stocker BD, Zscheischler J, Keenan TF, Prentice IC, Peñuelas J, Seneviratne SI. 2018. Quantifying soil moisture impacts on light use efficiency across biomes. *New Phytologist* **218**: 1430–1449.

Stocker BD, Zscheischler J, Keenan TF, Prentice IC, Seneviratne SI, Peñuelas J. 2019b. Drought impacts on terrestrial primary production underestimated by satellite monitoring. *Nature Geoscience* **12**: 264–270.

Sulman BN, Roman DT, Yi K, Wang L, Phillips RP, Novick KA. 2016. High atmospheric demand for water can limit forest carbon uptake and transpiration as severely as dry soil. *Geophysical Research Letters* **43**: 1–8.

Terashima I, Masuzawa T, Ohba H, Yokoi Y. 1995. Is photosynthesis suppressed at higher elevations due to low CO_2 pressure? *Ecology* **76**: 2663–2668.

Treydte KS, Frank DC, Saurer M, Helle G, Schleser GH, Esper J. 2009. Impact of climate and CO_2 on a millennium-long tree-ring carbon isotope record. *Geochimica et Cosmochimica Acta* **73**: 4635–4647.

Ubierna N, Farquhar GD. 2014. Advances in measurements and models of photosynthetic carbon isotope discrimination in C_3 plants. *Plant, Cell & Environment* **37**: 1494–1498.

Venables WN, Ripley BD. 2002. *Modern applied statistics with S. Fourth edition (Statistics and computing).* In: Chambers J, Eddy W, Hardle W, Sheather S, Tierney L, eds. New York, USA: Springer.

Verhoef A, Egea G. 2014. Modeling plant transpiration under limited soil water: Comparison of different plant and soil hydraulic parameterizations and preliminary implications for their use in land surface models. *Agricultural and Forest Meteorology* **191**: 22–32.

Voelker SL, Brooks JR, Meinzer FC, Anderson R, Bader MK-F, Battipaglia G, Becklin KM, Beerling D, Bert D, Betancourt JL *et al.* 2016. A dynamic leaf gas-exchange strategy is conserved in woody plants under changing ambient CO_2: evidence from carbon isotope discrimination in paleo and CO_2 enrichment studies. *Global Change Biology* **22**: 889–902.

Walker AP, Beckerman AP, Gu L, Kattge J, Cernusak LA, Domingues TF, Scales JC, Wohlfahrt G, Wullschleger SD, Woodward FI *et al.* 2014. The relationship of leaf photosynthetic traits – V_{cmax} and J_{max} – to leaf nitrogen, leaf phosphorus, and specific leaf area: a meta-analysis and modeling study. *Ecology and Evolution* **4**: 3218–3235.

Wang H, Prentice IC, Davis TW, Keenan TF, Wright IJ, Peng C. 2017a. Photosynthetic responses to altitude: an explanation based on optimality principles. *New Phytologist* **213**: 976–982.

Wang H, Prentice IC, Keenan TF, Davis TW, Wright IJ, Cornwell WK, Evans BJ, Peng C. 2017b. Towards a universal model for carbon dioxide uptake by plants. *Nature Plants* **3**: 734–741.

Weedon GP, Balsamo G, Bellouin N, Gomes S, Best MJ, Viterbo P. 2014. The WFDEI meteorological forcing data set: WATCH Forcing Data methodology applied to ERA-Interim reanalysis data. *Water Resources Research* **50**: 7505–7514.

Wingate L, Seibt U, Maseyk K, Ogée J, Almeida P, Yakir D, Pereira JS, Mencuccini M. 2008. Evaporation and carbonic anhydrase activity recorded in oxygen isotope signatures of net CO_2 fluxes from a mediterranean soil. *Global Change Biology* **14**: 2178–2193.

Wolf A, Anderegg WRL, Pacala SW. 2016. Optimal stomatal behavior with competition for water and risk of hydraulic impairment. *Proceedings of the National Academy of Sciences, USA* **113**: E7222–E7230.

Wright IJ, Reich PB, Westoby M. 2003. Least-cost input mixtures of water and nitrogen for photosynthesis. *American Naturalist* **161**: 98–111.

Wullschleger SD, Epstein HE, Box EO, Euskirchen ES, Goswami S, Iversen CM, Kattge J, Norby RJ, van Bodegom PM, Xu X. 2014. Plant functional types in Earth system models: past experiences and future directions for

application of dynamic vegetation models in high-latitude ecosystems. *Annals of Botany* **114**: 1–16.

Yi K, Maxwell JT, Wenzel MK, Roman DT, Sauer PE, Phillips RP, Novick KA. 2019. Linking variation in intrinsic water-use efficiency to isohydricity: a comparison at multiple spatiotemporal scales. *New Phytologist* **221**: 195–208.

Zhao M, Running SW. 2010. Drought-induced reduction in global terrestrial net primary production from 2000 through 2009. *Science* **329**: 940–943.

Zhou S, Duursma RA, Medlyn BE, Kelly JWG, Prentice IC. 2013. How should we model plant responses to drought? An analysis of stomatal and non-stomatal responses to water stress. *Agricultural and Forest Meteorology* **182–183**: 204–214.

Zhou S, Zhang Y, Williams AP, Gentine P. 2019. Projected increases in intensity, frequency, and terrestrial carbon costs of compound drought and aridity events. *Science Advances* **5**: 1–9.

Zhu Y, Siegwolf RTW, Durka W, Körner C. 2010. Phylogenetically balanced evidence for structural and carbon isotope responses in plants along elevational gradients. *Oecologia* **162**: 853–863.

Zuur AF, Ieno EN, Walker NJ, Saveliev AA, Smith GM. 2009. *Mixed effects models and extensions in ecology with R*. New York, USA: Springer.

Supporting Information

Additional Supporting Information may be found online in the Supporting Information section at the end of the article.

Dataset S1 Information about the 103 tree-ring sites used in the study; 5-year averaged values of environmental variables and of isotope-derived and predicted χ at each site; and original tree-ring chronologies with stable carbon isotope measurements used in the study.

Fig. S1 Impacts on the mean χ_{iso} levels and trends estimated from Eqn 3 of the selected values for the fractionation factors as a result of Rubisco carboxylation (*b*), photorespiration (*f*), post-photosynthetic processes (*d*) within their relative range of variation as reported in the literature.

Fig. S2 Elevation *z* (km) measured at each site when available vs those obtained from the WFDEI meteorological forcing dataset with 0.5° resolution (Weedon *et al.*, 2014).

Fig. S3 Yearly and monthly atmospheric CO_2 concentrations data from the Scripps Institution of Oceanography over 1951–2014 and 1958–2014, respectively.

Notes S1 Effect of including the mesophyll conductance term in the full discrimination model.

Notes S2 Estimation of β using the full formula of the least-cost hypothesis.

Notes S3 Estimating indices of radiation, evapotranspiration and plant-available moisture using SPLASH v.1.0.

Notes S4 Uncertainties related to the use of tree-ring $\delta^{13}C$ data as proxy of leaf-gas exchanges.

Notes S5 Coefficient value for the dependency of χ on elevation (*z*) in the linear regression model: difference between Wang *et al.* (2017) and the present study.

Table S1 Location of 103 tree-ring sites of the network with carbon isotopic measurements.

Table S2 Summary statistics for the environmental dependencies of logit χ_{iso} following different linear regression models: linear mixed-effects models and linear multiple models.

Please note: Wiley Blackwell are not responsible for the content or functionality of any Supporting Information supplied by the authors. Any queries (other than missing material) should be directed to the *New Phytologist* Central Office.